Space-Enhanced Solar Power for Equatorial Regions

Federica Bonetti[*], Colin R. McInnes[†]

ABSTRACT

This paper examines the concept of solar mirrors in a Earth orbit to provide solar farms with additional solar power during the hours of darkness. The design of the orbit is key for the purposes of the mission: the mirror needs continuous access to the Sun and the solar farm simultaneously. Therefore, orbits with high-eccentricity will be considered to increase the visibility time. Also, since the most convenient locations for solar power farms are about the equator, a suitable orbit should have a low inclination. This issue can be addressed through the concept of anti-heliotropic orbits that exploits mainly solar radiation pressure perturbations to generate highly-eccentric equatorial orbits able to maintain the orientation with respect to the Sun. The considered configuration consists in two space mirrors in a flower constellation rotating with the Earth to deliver a repeat ground track.

INTRODUCTION

This paper discusses the use of orbiting mirrors to improve the efficiency of large-scale terrestrial solar power farms. Placing mirrors in space, in a convenient orbit around the Earth, would make it possible to reflect sunlight downwards. The reflected sunlight needs to point towards a specific location on the ground where a series of large collectors will benefit from this surplus energy for terrestrial use. It is estimated that the use of space mirrors for terrestrial solar power generation could potentially reduce the cost of solar electric power to less than 6 cents per kWh[1] .

Initial ideas on the prospect of beaming sunlight from space towards the Earth were proposed in 1978 by Ehricke in Reference 2. The project, Power Soletta, entailed a constellations of 3 mirror-satellites in an Earth orbit at $4200 \ km$ altitude. However, because of the choice of the orbit, in order to reproduce normal daylight solar intensity (brightness equal to 1 solar constant) each mirrors would have an area of $4617 \ km^2$. Given a solar flux of $1362 \ W/m^2$, a thin-film mirror with a area density of $10 \ g/m^2$ delivers a huge power density of $130 \ kW/m^2$.

The choice of reflector's orbit is critical to determine the time of the day when the additional energy is provided and the duration of the contact with the solar farm. For example, interesting strategies would be to reflect sunlight in the evening and early morning hours[3] or, in general, during the night or at least during peak hours (evening). The ideal solution would be to have a space mirror that sees the Sun and the solar farm for the greatest duration.

[*]email: F.Bonetti.1@research.gla.ac.uk; School of Engineering, University of Glasgow, Glasgow, G12 8QQ
[†]email: Colin.McInnes@glasgow.ac.uk; School of Engineering, University of Glasgow, Glasgow, G12 8QQ

Therefore, initial concepts consider polar Sun-synchronous orbits so that the mirror would never be in eclipse. However, in this case, the maximum time in view of the ground site is as low as 9 minutes, or, at most, 20 minutes if the solar mirror is able to steer, changing its attitude, in order to track the solar farm while it is visible. For this reason, more complex designs are considered, for example, a constellations of 18 satellites is designed in Reference 3. Since it is not possible to have continuous access to a single location, these satellites would serve 40 evenly distributed terrestrial solar farms.

Clear locations are more suitable for this strategy so that it is possible to avoid frequent cloud coverage. For this reason, the equatorial regions are the most appealing and, even if Sun-synchronous polar orbits would allow continuous reflection of sunlight, it is rather straightforward to note that polar orbits would not be the most immediate choice. Another family of orbits, heliotropic orbits, can also be considered for this purpose. Heliotropic orbits are eccentric orbits that, balancing J_2 and solar radiation pressure (SRP) perturbations, generate quasi-frozen orbits able to track the Sun (or frozen orbits in the case of perfectly equatorial orbits). These orbits present an interesting option for space solar power, where their analytical description and derivation can be found in Reference 4. In this paper, taking into account the concept of heliotropic orbits, highly-eccentric equatorial orbits able to track the Sun will be considered to increase the time in view of the space mirror and to deal with SRP and J_2 perturbations. Moreover, the steering law for the solar mirror to track the solar farm on the ground, while it is visible, will generates oscillations in the SRP perturbation. For this reason, the family of frozen orbits investigated in this paper will slightly differ from those found in Reference 4.

The goal of this specific work is to provide a daily surplus solar energy for at least 3 locations situated near the equator. Therefore, the key issue is to generate an orbit with repeat ground track.

This subject has been extensively investigated in the past and most orbital constellations have been developed around this concept. For example, in 1981, The San Marco Project conceptualized the "Sistema Quadrifoglio" as an equatorial constellation of four satellites in Reference 5. In this concept, each satellite spends about 6 hours near the orbit apogee and two hours in transition between successive apogees. Due to the phasing of satellites in the orbits, 3 of the satellites are always near apogee and the other is in transition to replace the spacecraft with the largest mean anomaly. The three spacecraft near apogee (about $120°$ apart) have line of sight visibility of each other and each can observe well over $1/3$ of the Earth's surface. This new way to design satellite constellations has stimulated interesting subsets such as the "shape-preserving" constellation. The "Sistema Quadrifoglio" generated the basis of Flower Constellations, which can be set so that each satellite of the constellation has identical repeat ground tracks. In this paper a flower constellation of two mirror-satellites (technically an "incomplete" flower constellation) has been designed to accomplish the goal of providing surplus solar energy to 3 large solar farms in Central Africa, America and Oceania.

In the first section, the design of the orbit is described in detail. In particular, in the first subsection, the most suitable flower constellation is considered and the required semi-major axis is estimated. In the second subsection,

2

the process used to evaluate the correct value for the eccentricity is reported. The "anti-heliotropic" condition is achieved exploiting SRP and J_2 perturbations taking into account also the eclipse time. In the following subsections two steering laws are considered for the space mirror: the first entails the mirror always pointing at the centre of the Earth, whereas according to the second steering law the exact position of the solar farm is tracked while the mirrors are visible. Finally the last section investigates the power generated by each solar farm and, moreover, a detailed description of the loss factors is reported.

DESIGN OF THE ORBIT

Flower Constellation

The Flower Constellation (FC) takes its name from its shape as seen in the Earth rotating reference frame (ECEF). The parameters that describes a FC are the number of petals (N_p), the number of sidereal days to repeat the ground track (N_d), the number of satellites (N_s) and four other parameters that determine the phasing of the constellation: the node identification (F_n), the phasing step (F_h), and finally the RAAN (Ω) and the mean anomaly (M) of the constellation.[6] The other orbital parameters (argument of perigee (ω), inclination (i), semi-major axis (a) and eccentricity (e)) should be the same for all mirrors. However, for the purposes of this work, the anti-heliotropic condition needs to be maintained for each mirror of the constellation and, for this reason, the orbits are slightly different from each other. The FCs are characterized by an axis of symmetry that can be arbitrarily oriented. When the FC's axis of symmetry is aligned with the Earth's spin axis, the mirror shows identical repeated ground tracks[7] . The condition to satisfy in order to achieve a repeat ground track is given by:

$$T_r = N_p T = N_d T_G \tag{1}$$

where T_r is the period of repetition, T_G is the Greenwich nodal period and T is the anomalistic period, i.e. the time necessary to complete one petal of the flower constellation. In order to obtain a repeated orbit T has to satisfy the relationship in Eq. (1) and, thereafter, the semi-major axis can be evaluated from this. The design process of a specific FC starts with the choice of the parameters to describe the constellation, the generation of a complete FC and then the selective elimination of those satellites (mirrors in this case) unnecessary for the final purpose of the mission. The objective is to provide each day additional solar energy for 3 solar farms near the equator. Therefore, as for the "Sistema Quadrifoglio"[5] , the parameters of the suitable FC are set as follow: $N_p = 3$, $N_d = 1$ and $N_s = 4$. Then, through Eq. (1), the anomalistic period has to be approximately 8 hours and a semi-major axis of $20270.4\ km$ follows. The considered areas are situated in Central Africa, the Pacific coast and Oceania. In order to track these three areas,

the phasing rules of the constellation are chosen so that RAAN and mean anomaly are given by:

$$\Omega = [0 \ \ 180 \ \ 360 \ \ 540]° \qquad M = [0 \ \ 1260 \ \ 2520 \ \ 3780]° \tag{2}$$

The last parameter required to complete the design of the constellation is the eccentricity. The mirrors are high area-to-mass ratio objects and so the effects of SRP (and J_2 perturbations) would make the mirrors largely deviate from a Keplerian trajectory. In the next section the effect of these perturbations on the orbits is quantified and, in particular, the perturbations are exploited to estimate a suitable eccentricity and therefore achieve a Sun-following condition.

RAAN and mean anomaly determine the position of the orbit with respect to the Sun while the eccentricity only regulates the shape of the orbit. For this reason, it is already possible to make some distinctions between the four orbits of the mirrors: considering the position of the Sun with respect to the mirrors of the flower constellation, there are two of them, termed "day" mirrors, whose apogee is always in sunlight and other two orbiting near the apogee while they are in the dark, termed "night" mirrors. Figure 1 shows the complete flower constellation in the inertial reference frame (ECI) when a nominal eccentricity value of 0.5 is chosen. In particular, the day-mirrors follow the black orbits and the night-mirrors follow the grey orbits. For the purposes of this paper, the night-mirrors are of most interest, therefore the day-mirrors are removed from the constellation and only the other two orbits will be further investigated. In particular, the incomplete flower constellation entails the two mirrors with $\Omega = [0° \ \ 540°]$ and $M = [0° \ \ 3780°]$.
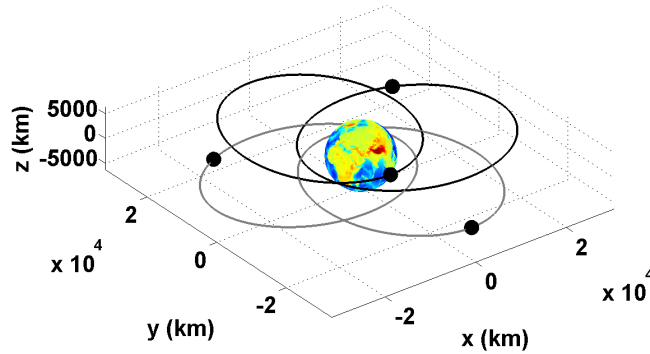

Figure 1. Complete flower constellation with eccentricity 0.5 in the inertial reference frame (ECI).

Anti-heliotropic Orbits

Large space mirrors are high area-to-mass ratio objects so that SRP (and oblateness perturbation) are no longer negligible[4] . These perturbations can be exploited to generate new families of highly perturbed non-Keplerian orbits.[4, 8]

Specifically, in Reference 4, a simplified planar model of the dynamics is investigated through the Hamiltonian of the system and novel families of equilibrium in-plane orbits are identified: heliotropic and anti-heliotropic orbits, where, choosing suitable combinations of semi-major axis and eccentricity, a Sun-synchronous condition is achieved passively and the other in-plane orbital elements are constant. The former are Sun-pointing apogee orbits and entail that the mirror would be in sunlight while near the apogee. The second family of orbits generated from this analysis are Sun-pointing perigee orbits. In this case, the mirror would spend most of the time over the dark side of the Earth. Since the goal is to provide additional solar energy during the night or early morning and evening hours, the second family of orbits are of most interest. With respect to the analysis of the planar model investigated in Reference 4, in this paper, the eclipse effect and the SRP perturbation due to the steering of the mirror to track the solar farm are considered during the investigation of the orbital elements through the Lagrange equations.

The orbits considered have zero inclination and the ecliptic obliquity is neglected so that it is necessary to investigate only the in-plane motion. Moreover, as in Reference 9, the normal to the surface of the mirror is assumed within the ecliptic plane so that SRP perturbs only the in-plane motion. In these conditions, as in Reference 9 only three osculating orbital elements are required in order to describe the resulting trajectory, which can be expressed through the Lagrange Equations:

$$\frac{da}{df} = \frac{2pr^2}{(\mu(1-e^2))^2} \left[e\,sin(f)R + \frac{p}{r}T \right] \tag{3}$$

$$\frac{de}{df} = \frac{r^2}{\mu} \left[sin(f)R + \left(1 + \frac{r}{p}\right) cos(f)e\,\frac{r}{p}T \right] \tag{4}$$

$$\frac{d\omega}{df} = \frac{r^2}{\mu e} \left[-cos(f)R + \left(1 + \frac{r}{p}\right) sin(f)T \right] \tag{5}$$

where R and T are the radial and transverse components of the perturbations which the mirror is subject to. Differently from Reference 4, in this work also the J_2 perturbation experienced by the mirror is considered and can be written as follow[10] :

$$a_{J_2} = \frac{3}{2} \frac{\mu}{r^4} R_e^2 \, J_2 \, R \tag{6}$$

where R_e is the Earth's radius and J_2 is the oblateness parameter (1.083×10^{-3}). Since the mirror needs to steer in order to track the solar farm while in visibility, its relative orientation with respect to the Sun is one-day periodic, but it changes along the orbit. As consequence, the SRP perturbation varies according to the steering law.

Moreover, from the theory of the umbra cone[11] , the true anomalies identifying the beginning and end of the eclipse can be determined through geometrical considerations. Considering the umbral geometry described in Figure 2, it is possible to compute the vector δ, i.e. the vector originating at the umbral cone axis, pointing to the spacecraft at the projected spacecraft location, at the time t. The true anomalies identifying the eclipse are those that satisfy the following condition: $|\boldsymbol{\delta}(f)| = \xi(f)$, where ξ is the distance between the umbral cone axis and the umbra terminator

point at the projected spacecraft location and is given by:

$$\xi = (\chi_u - |\mathbf{r_s}|)\, tan(\alpha_u) \tag{7}$$

In Eq. (7), χ_u is the distance between the umbral cone apex and the centre of the Earth and, as can be seen in Figure 2, $\mathbf{r_s}$ is the projection of the position vector of the mirror in ECI ($\mathbf{r_{ECI}}$) on the unit solar vector ($\hat{s}$). Thus, the true anomalies identifying the eclipse along an orbit with semi-parameter p and eccentricity e are obtained through the following equation:

$$f_{ecl_{1,2}} = \pm arcos\left(-\frac{2p - \chi_u\, tan(\alpha_u)}{p - e\,\chi_u tan(\alpha_u)}\right) \tag{8}$$

where subscripts 1, 2 stand for the beginning and the end of the eclipse, respectively. In order to take the eclipse duration into account, the piecewise integrals of the three orbital parameters in Eqs. (3-5) averaged over one orbital period are considered.

In the next sections, two steering laws are investigated: an Earth-pointing steering law and a solar-farm-tracking steering law. The Earth-pointing steering law can be obtained analytically, whereas a numerical investigation is performed to obtain the second steering law. The steering law of the mirror is used to estimate the SRP perturbation along the orbit and the consequential variation of the orbital parameters through Eqs. (3-5).
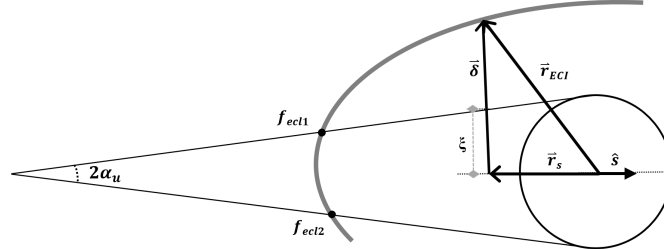

Figure 2. Geometry of the umbral cone caused by the Earth on the orbit of the mirror.

Earth-Centre Pointing Steering Law

The first steering law investigated is an Earth-centre pointing strategy, i.e. the mirror points always towards the centre of the Earth. Considering Reference 9, where a Moon-centre pointing law is developed, and the geometry shown in Figure 3, the angle γ can be written as a function of the true anomaly f as follows:

$$\gamma = \frac{\alpha}{2} = \frac{\pi - f}{2} \tag{9}$$

6

where α is the angle between the incoming and reflected rays measured at the mirror (Figure 3). Thus, the acceleration perturbation due to solar radiation pressure can be written as[9] :

$$a_{SRP}(f) = P_{SRP}\, C_r \frac{A_{sun}}{m} sin^2 \left(\frac{f}{2}\right) \left[sin \left(\frac{f}{2}\right) R + cos \left(\frac{f}{2}\right) T\right] \tag{10}$$

where P_{SRP} is the solar pressure at $1\ AU$ equal to $4.56 \times 10^{-6}\ N/m^2$ [4] , C_r is the reflectivity coefficient given by $1 + r$ where r is the reflectivity of the material set to 0.9 (generally aluminium)[12] and A_{sun} is the area of the mirror exposed to the Sun. Considering Eq. (6) and Eq. (10) in Eqs. (3-5), the piecewise integrals can be written as:

$$\Delta a_{ECL} = \int_0^{f_{ecl_1}} \frac{da}{df}df + \int_{f_{ecl_1}}^{f_{ecl_2}} \frac{da_{J_2}}{df}df + \int_{f_{ecl_2}}^{2\pi} \frac{da}{df}df \tag{11}$$

$$\Delta e_{ECL} = \int_0^{f_{ecl_1}} \frac{de}{df}df + \int_{f_{ecl_1}}^{f_{ecl_2}} \frac{de_{J_2}}{df}df + \int_{f_{ecl_2}}^{2\pi} \frac{de}{df}df \tag{12}$$

$$\Delta \omega_{ECL} = \int_0^{f_{ecl_1}} \frac{d\omega}{df}df + \int_{f_{ecl_1}}^{f_{ecl_2}} \frac{d\omega_{J_2}}{df}df + \int_{f_{ecl_2}}^{2\pi} \frac{d\omega}{df}df \tag{13}$$

where da_{J_2}, de_{J_2} and $d\omega_{J_2}$ are the perturbations of a, e and ω due only to the Earth's oblateness because there is not SRP perturbation while the mirror is in eclipse. Every mirror completes 3 orbits everyday and experiments the eclipse only once per day. Therefore, the perturbations are one-day periodic and Eqs. (11-13) are valid only for the orbit during which the eclipse occurs. In order to estimate the variation of the orbital parameters for the other two orbits the piecewise formulation is not necessary because SRP and J_2 perturbs the orbit continuously. Therefore, the overall variation of the orbital parameters averaged over one day (T_G is the Greenwich nodal period) can be written as:

$$\Delta a_{day} = \frac{1}{T_G} \left[\Delta a_{ECL} + \int_0^{4\pi} \frac{da}{df}df\right] \tag{14}$$

$$\Delta e_{day} = \frac{1}{T_G} \left[\Delta e_{ECL} + \int_0^{4\pi} \frac{de}{df}df\right] \tag{15}$$

$$\Delta \omega_{day} = \frac{1}{T_G} \left[\Delta \omega_{ECL} + \int_0^{4\pi} \frac{d\omega}{df}df\right] \tag{16}$$

Thus, substituting Eqs. (11-13) in Eqs. (14-16), the daily variation of semi-major axis, eccentricity and argument of perigee can be estimated for the orbits of the space mirrors. As expected, Δa_{day} and Δe_{day} are equal to zero, therefore, the one-day averaged J_2 and SRP perturbations do not affect the semi-major axis and the eccentricity of the orbit even when the eclipse is considered. A similar problem was already investigated without J_2 perturbation in Reference 9, the same result was expected because of the periodicity of the J_2 perturbation along the orbit.
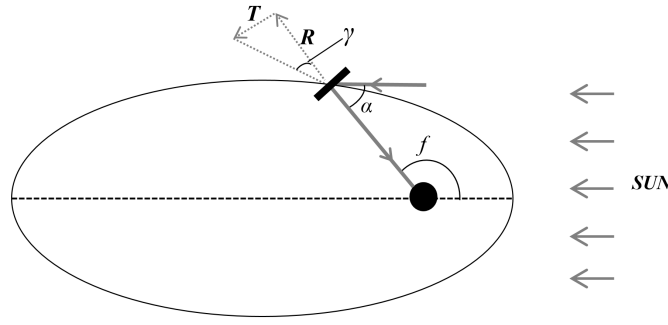
Figure 3. Geometry showing the relative position of the mirror and the Earth for the first steering law.

Moreover, $\Delta\omega_{day}$ is developed as well from Eq. (16) and, as expected, the summations is different from zero. SRP and J_2 perturbations generate the precession of the perigee. This effect can be exploited to estimate the eccentricity of the orbit so that a Sun-following condition is achieved. The condition considered to obtain the eccentricity of the orbit is given by this expression: $\Delta\omega_{day} = \dot{\lambda}_s$. This condition is required to precess the orbit's apse line at the same rate as the Sun ($\dot{\lambda}_s = 0.9856°/day$)[13] . Through this procedure and given the area-to-mass ratio of the mirror the eccentricity of the orbit can be estimated. In Figure 4 the eccentricity is estimated for several values of the area-to-mass ratio of the mirror for two different values of the semi-major axis: $20270.4\ km$, associated with the considered flower constellation (FC) ($N_p = 3,\ N_d = 1$) and $26561.7\ km$ associated with a FC of $12\ h$ ($N_p = 2,\ N_d = 1$) period that would have been the second choice. However, the second FC has been excluded because it would have been able to provide sunlight only for two solar farms, also, the chosen FC provides more flexibility. As can be noted, not all the combinations are possible, also the eccentricity has an upper limit (e_{max}) of $1 - \frac{R_e + 1000}{a}$ in order to avoid perigee heights below $1000\ km$. Since a high time of visibility near the apogee and, therefore, a large eccentricity is crucial for the purposes of the mission, only values of the eccentricity above 0.4 (e_{min}) are considered. This information is used to select the feasible range of area-to-mass ratio values for the mirrors: $\left(100 \leq \frac{A}{m} \leq 160\right)\ m^2/kg$. In order to have these values of area-to-mass ratio the space mirror needs to be four times lighter than the L'Garde Sunjammer developed by NASA. Sunjammer has a solar sail loading[14] of $26.6\ g/m^2$ (σ_s), otherwise a mass density of $(6.25 - 10)\ g/m^2$ is required to achieve the range of eccentricities of interest and, therefore, the Sun-following condition. It is expected that in future performance of space mirrors and solar sails will be improved, for example by substituting Kapton substrates with advanced materials. This variation would make the manufacturing of ultralight space mirrors feasible by decreasing their weight of 10-12 times. When this steering law is considered, every orbit of the flower constellation has the same eccentricity.
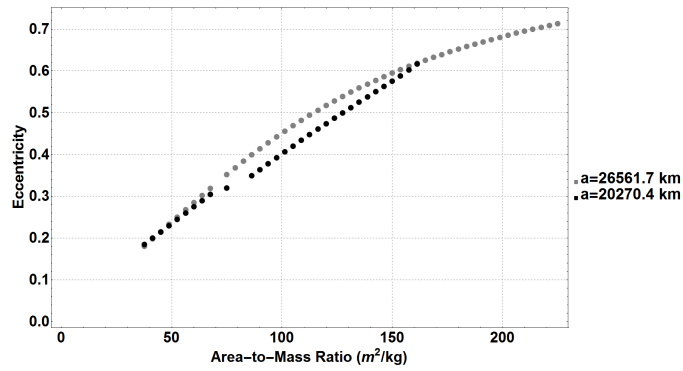
Figure 4. Combination of eccentricity and area-to-mass ratio values that satisfy the Sun-following condition for the first steering law.

Second Steering Law: Tracking of the Solar Plants

With respect to the Earth-centre pointing strategy, the second steering law is very specific for the objective of this paper. Every time the mirror is near the apogee and in visibility for one of the solar farms, it will steer to track it. Contrarily to the first steering law described in the previous section, in this case a different law as well as an eccentricity is estimated for each mirror in order to achieve the Sun-following condition for all of them. It is important to highlight that the control laws of the mirrors need to maintain symmetry along the orbit so that the averaged variation of semi-major axis and eccentricity due to the perturbations (Eqs. (14-15)) is kept equal to zero as in the previous case. In order to achieve a reasonable symmetry, the position of the solar farm needs to be exactly under the apogee of the orbit. The selected locations for the three solar power farms are summarized in Table (1). It is necessary that the solar farms are equidistant from each others in order to assure that the surplus solar energy is received during the night, for this reason two of the locations considered are necessarily in the sea. Despite this result can be considered an issue, it is actually convenient that this technology is developed far from urban areas in order to minimize the effects on the population. Moreover, if a specific area that is not exactly on the equator needs to be targeted, inclined orbits should be considered and the 3D dynamics needs to be investigated. Inclined orbits provides larger flexibility for the strategy design.

Table 1. Location of the chosen solar power farms.

	Pacific Coast	Central Africa	Oceania
longitude	$92\,W$	$30\,E$	$149\,E$
latitude	0	0	0
Time	$GMT - 3h$	$GMT + 1h$	$GMT + 8h$

The values of RAAN and mean anomaly employed are those found previously for the night-mirrors ($n°1$ and $n°4$),

9

also, the initial argument of perigee of the orbits (ω) is set to $270°$. Finally, an area-to-mass ratio equal to $150\ m^2/kg$ ($\sigma_s = 6.67\ g/m^2$) is considered. During the search of the eccentricity, the geometry in Figure 5 is used to estimate the nadir angle (η) measured at the mirror from the sub-satellite point to the target, i.e. the solar farm[15] . The minimum elevation angle (see Figure 5) that is considered for the mirror is $\epsilon_{min} = 24°$: this value is chosen so that the hypotheses made are valid, such as the value for the atmospheric transmittance. Taking into account the angular Earth's rotation (velocity of rotation ω_e), the geographical coordinates of the solar farms are written as $(lon + \omega_e t, lat)$.
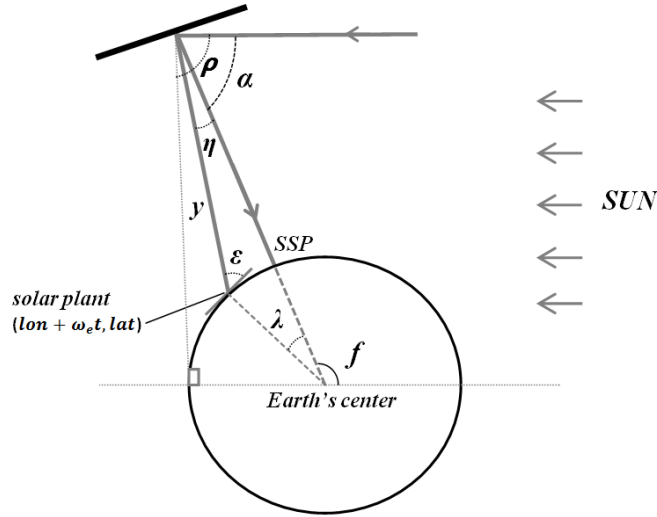

Figure 5. Geometry of the the mirror with respect to the solar farm for the second steering law.

Since the position of the sub-satellite point (SSP) and the target are known, it is possible to estimate the value of the Earth central angle (λ) and the Earth angular radius (ρ) (see Reference 15 and Figure 5). After that, the nadir angle is defined as follow:

$$tan(\eta) = \frac{sin(\rho)sin(\lambda)}{1 - sin(\rho)cos(\lambda)} \tag{17}$$

Once the angle η is known, similarly to the case before, the angle describing the orientation of the mirror (γ) can be written as a function of the true anomaly f and η:

$$\gamma = \frac{\alpha'}{2} = \frac{\pi - f + \eta}{2} = \frac{\pi - f'}{2} \tag{18}$$

Equation (10) can still be used to compute the solar radiation pressure perturbation in this case by substituting f with $f + \eta$. The mirror steers to track the solar farms while it is in visibility, i.e. for elevation angles larger than ϵ_{min}. In order to keep a fair symmetry for the overall SRP perturbation, each mirror tracks all the three solar farms once per day, in this way the resulting eccentricities are quite similar. Moreover, passage it occurs during the day.
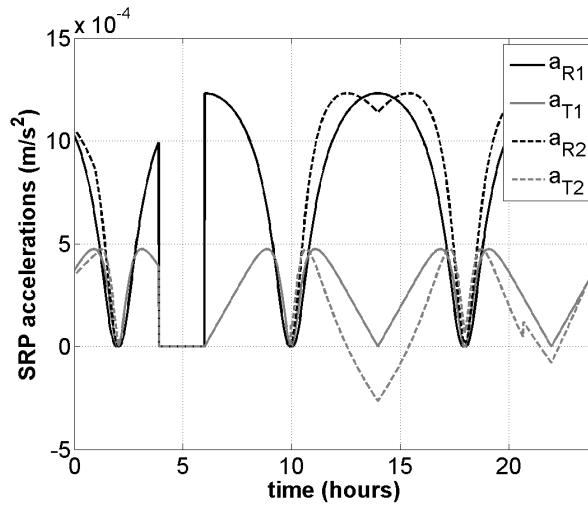
10

Figure 6. Daily variation of the acceleration due to solar radiation pressure provided when the first (continuous line) and the second (dashed line) steering laws are applied.
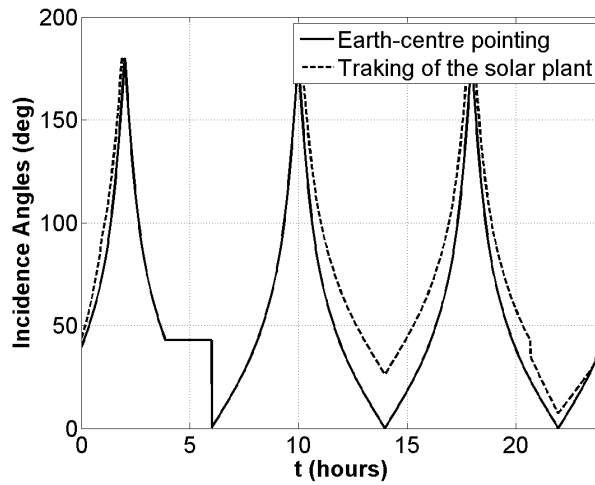

Figure 7. Daily variation of the incidence angles for the two steering laws.

Under these conditions, as for the previous case the Lagrange equations are used to compute the variation of the orbital parameters. Again, the summation in Eqs. (14-15) is computed. The variation of the semi-major axis and the eccentricity are negligible since their values oscillate periodically over one day. Computing Eq. (16), it can be proved that a precession of the perigee occurs. Therefore, as before, the condition $\Delta\omega_{day} = \dot{\lambda}_s$ is employed to estimate the eccentricities for the orbits of the night-mirrors. The obtained values are given by $e_1 = 0.58$ and $e_2 = 0.50$, respectively. Moreover, the acceleration along the directions **R** and **T** (see Figure 5) due to the solar radiation pressure for the two steering laws is reported in Figure 6. As expected, the curves are rather similar and sometimes there is not any difference. Finally in Figure 7 the angles α (continuous line) and α' (dashed line) are reported. Again, as

11

expected, the curves are comparable, to track the solar farms only small variations with respect to the Earth-centre pointing steering law are required.

Anti-heliotropic Flower Constellation for Space Reflectors

The second steering law described in the previous section allowed for the estimation of the eccentricity of the orbits exploiting J_2 and SRP perturbations and satisfying the Sun-following condition. In particular the night-mirrors, i.e. those mirrors having the apogee always in the opposite direction with respect to the Sun, are considered so that the anti-heliotropic condition is achieved. This can be demonstrated if the apparent motion of the Sun's path around the Earth, due to the Earth's rotation on its axis, is considered.

The orbits of the night mirrors assemble the flower constellation which can be visualized in the rotating frame in Figure 8 and in the inertial frame in Figure 9. The ground track and the coverage[15] of the constellation can be found in Figure 10, where it can be seen that the mirrors orbit over the three places of interest when they are at the apogee of every orbit. It is important to underline that the solar power farms have to be exactly below the apogee of the orbit to have symmetric SRP perturbation during the tracking of the solar farm so that the variations of the semi-major axis and the eccentricity oscillates around the Keplerian value.
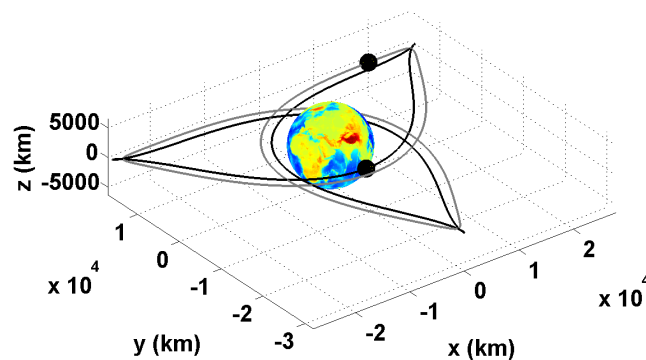

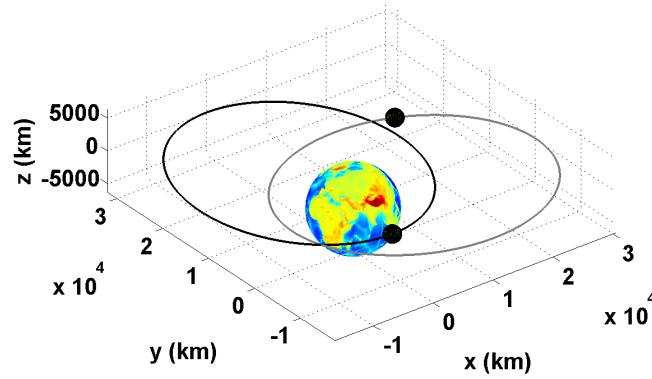**Figure 8. Flower Constellation of the night-mirrors in the rotating Earth-centred reference frame (ECEF).**

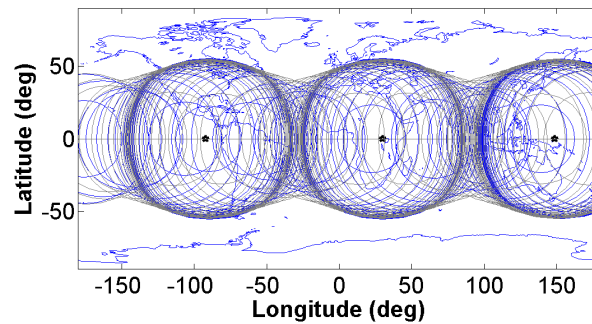**Figure 9. Flower Constellation of the night-mirrors in the inertial Earth-centred reference frame (ECI).**

Figure 10. Ground Track and coverage (for $\epsilon > 24°$) of the two mirrors (black line for the first mirror with $\mathrm{RAAN} = 0°$, $\mathrm{M} = 0°$ and grey line for the second mirror with $\mathrm{RAAN} = 360°$, $\mathrm{M} = 360°$).

Considering a minimum elevation angle of $24°$ (see geometry in Figure 5), the time of visibility of each mirror over the solar farm is roughly between 6 and 7 hours. This can be seen in Figure 11 and 12, where the reference time is Greenwich Mean Time (GMT) and the time difference for each location is considered to determine the local time when the surplus energy is provided (see Table (1)). Therefore, considering the local time in the three locations, the strategy can be summarized as follow: the first mirror ($RAAN = 0°$, $M = 0°$) tracks the first solar farm in central Africa between 1.40 AM and 8.30 AM, the second solar farm (Pacific Coast) from 5.30 AM to 12.20 PM and the third solar farm in Oceania between 00.30 AM and 6.45 AM; whereas, the second mirror ($RAAN = 360°$, $M = 360°$) tracks the first solar farm between 7.50 PM and 2.20 AM, the second one between 11.40 PM and 6.10 AM and the

13

third solar farm from 6.40 PM to 1.12 AM. The eclipse time for the two mirrors is around $2-2.5\ h$ and it occurs while the first mirror is orbiting over the first solar farm and when the second mirror is above the second solar farm.
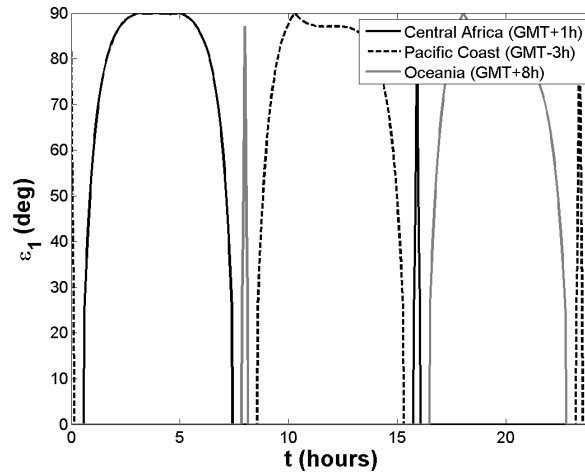

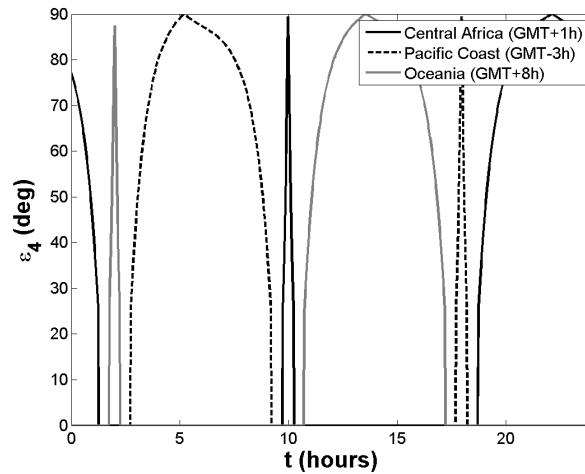**Figure 11. Daily elevation angle of the first mirror over the three locations considered for the power farms.**

Figure 12. Daily elevation angle of the second mirror over the three locations considered for the power farms.

It is interesting to highlight that in some cases the coverage occurs during the day (see mirror 1 over the Pacific coast), although the Sun would provide solar power anyway, the process would be improved because the mirrors would act as concentrators of solar energy. More details about the employed strategy are reported in Table (2) which shows that the total coverage time is $11\ h$ for the solar farm in Central Africa, $10\ h\ 55'$ for the Pacific coast and $13\ h\ 13'$ for the third solar farm in Oceania. The third solar farm has a larger coverage because no eclipse occurs while the mirrors orbit above it.

14

Table 2. Adopted strategy for the coverage of the solar farms during the night, evening or early morning.

# Mirror	Solar Plant	Time-Range Coverage	Eclipse	Total Time Coverage
1	Central Africa	$1.40\ AM - 8.30\ AM$	$2h\ 21'$	$4h\ 28'$
1	Pacific Coast	$5.30\ AM - 12.20\ PM$	0	$6h\ 43'$
1	Oceania	$00.30\ AM - 6.45\ AM$	0	$6h\ 16'$
2	Central Africa	$7.50\ PM - 2.20\ AM$	0	$6h\ 33'$
2	Pacific Coast	$11.40\ PM - 6.10\ AM$	$2h\ 05'$	$4h\ 12'$
2	Oceania	$6.40\ PM - 1.12\ AM$	0	$6h\ 30'$

Control Attitude and Shape of the Reflector

As in Reference 12, a control moment gyro (CMG) is considered for the attitude control of the mirrors. The CMG would provide the higher torque necessary to stabilize the mirrors during the initial maneuvers and for the attitude control necessary to track the solar farms on the ground. Also, a low thrust propulsion system should be considered as well mainly in order to periodically control the attitude while the CMG is saturated and for station keeping. It is important to highlight that because of the high orbit considered, the effect of the atmospheric drag is completely absent. This method is taken into account in Reference 12 to control the attitude of mirrors with a diameter of $1\ km$. A larger space mirror can be considered a modular structure made of several $1\ km$-mirrors.

Another interesting option is the use of electrochromic layers to effectively control the attitude of the mirror. The reflectivity of the surface would be locally different generating a torque that can be exploited to passively control the attitude of a large mirror. The electrochromic layers should be on the edge of the mirror in order to not affect the collection of solar power. Electrochromic coatings have been successfully employed on the IKAROS solar sail for attitude control in 2010 [16].

Finally, another important issue to deal with is the shape of the mirror. In Reference 9, it can be seen that advantages are provided when a parabolic mirror is employed. The area of the illuminated spot on the ground is very large (order of magnitude $10^8\ km^2$ with a flat mirror) and, in general, the area covered by the solar farm is smaller than the overall available area. Thus, the energy reflected outside the area of the solar farm is lost. A parabolic mirror would concentrate the reflected sunlight over a smaller area therefore reducing the loss of energy. Because of the large distance between the mirror and the solar farm, a very moderate curvature of the mirror would be required to provide greatly improved performances.

To obtain a parabolic mirror, a good option is found in Reference 17, where the surface of a thin slack circular film is employed to investigate the possibility of a shape-controlled space mirror. Although it is shown that the nominal deflection shapes due to the effect of SRP are non-parabolic, through an inverse method, the reflectivity distribution necessary to create a true parabolic deflection profile is derived analytically. The required distribution

for the reflectivity could be provided through the suitable modification of the film surface. However, the change in reflectivity would cause a loss in the collected solar energy that should be considered in the computation of the overall energy provided.

In order to maximize the effect of a parabolic mirror, it is necessary to adjust the focal distance along the orbit so that the solar radiation is always concentrated on the solar farm. Therefore, an adjustable parabolic surface should be considered. It follows from the previous discussion about the reflectivity pattern in Reference 17 that if the distribution of reflectivity over the surface of the mirror is adjustable the focal distance can be modified. This concept could be achieved in principle through the use of electrochromic materials.

COMPUTATION OF THE ENERGY PRODUCED

In the previous section the constellation designed was described in detail. Two mirrors in eccentric orbits provide three locations on the ground with additional solar energy during the night or the evening hours (peak times). In this section the solar power generated from the solar farms is calculated also taking into account the loss effect of the eclipse. Considering the reflection of light from the mirror over the Earth's surface, the image of the Sun that is reproduced over the surface at a distance y (see Figure 5) from the mirror (slant range) according to Reference 9 can be written as:

$$A_i(t) = \frac{\pi}{4sin(\epsilon(t))}(D_m^2 + y^2\beta^2) \tag{19}$$

where D_r is the diameter of the mirror, ϵ is the elevation of the mirror above the horizon with respect to the location of the solar power farm, and β is the solid angle subtended by the Sun. β is obtained geometrically computing the ratio of the Sun's diameter over the Sun-Earth distance and is given by 0.0093 [18]. However, as in Reference 9, it can be shown that if a parabolic mirror is considered better performances are achieved. The Sun's image projected over the Earth's surface by a parabolic mirror can be written as:

$$A_p(t) = \frac{\pi}{4sin(\epsilon(t))}y^2\beta^2 \tag{20}$$

in this case y is also the focal distance. As said in the previous section, the parabolic mirror is assumed to be made of electrochromic materials that modify the reflectivity distribution over the surface of the mirror and change the focal distance as required. Thus, accounting for all significant losses as in Reference 12, the total power P_m delivered by the mirror can be written as follow:

$$P_m = \mu\rho\tau\psi I_0\frac{A_m}{A_{i,p}}cos\left(\frac{\alpha}{2}\right) \tag{21}$$

where μ is the flatness coefficient of the reflecting surface, ρ is the reflectivity coefficient, τ is the atmospheric trasmissivity, ψ is the cloud cover coefficient and $\frac{\alpha}{2}$ is the angle of incidence that describes the geometry between Sun and

mirror (see Figure 5). Also, I_0 is the solar constant given by $1.37\ GW/km^2$ [3] . The power received at the ground depends on the dimensions of the solar farm. If the solar farm is as big as the illuminated spot (Eq. (20) for a parabolic mirror), the maximum power achievable would be received. Therefore, the power received at the ground is given by the product of the power reflected by the mirror and the area of the solar farm (A_{SF}). If the losses due to the PV array modules (ϵ_{PV}) and the ground coverage ratio (ϵ_{GCR}) are considered, the total power provided is given by:

$$P_{tot} = P_m\ \epsilon_{PV}\ \epsilon_{GCR}\ A_{SF} \tag{22}$$

All loss factors are described in detail in the next section. Finally, the total energy produced (GWh) by each solar farm is given by:

$$E_{tot} = \frac{\int_0^{1\ day} P_{tot}\ dt}{1\ hour} \tag{23}$$

Loss Factors

As seen in the previous section, losses combine to reduce intensity and they have to be considered to estimate the energy collected by the solar farm. Some losses are due to the quality of the mirror and the efficiency of the solar farm and others are associated with natural conditions. The mirror flatness (μ) indicates the presence of wrinkles on the surface of the mirror. In particular, deep wrinkles with steep slopes disperse sunlight off the considered illuminated spot, otherwise, although shallower wrinkles disperse only some light off the target, the overall light impinging upon the illuminated spot may be dispersed unevenly. For this reason as well as for manufacturing purposes, the use of smaller mirrors to build a large reflecting surface is advised in order to average out dispersions from wrinkles. The root-mean-square (RMS) edge gradient of the surface of the membrane is estimated to be approximately $\sigma = 0.0002\ rad$ [12] . According to Reference 12, the linear dispersion of the image (d_{im}) resulting from imperfections of the membrane can be computed through Eq. (24).

$$d_{im} = 2\sigma y \tag{24}$$

where y is the slant range. Considering Eq. (24), the illuminated spot on the ground with the additional spill-over area caused by the dispersion is given by:

$$A_{tot} = \pi \left(\frac{D_s + d_{im}}{2}\right)^2 \tag{25}$$

Thus the flatness coefficient, indicating the loss in intensity due to surface wrinkles, can be written as:

$$\mu = \frac{A_{tot}}{A_i} \tag{26}$$

Assuming, for example, a mirror of diameter $8\ km$ (roughly $A_m = 50\ km^2$), the area of the illuminated spot over the solar farm in central Africa, for example, is given by $5164\ km^2$, the average spill-over area due to the dispersion is

1.34 km; therefore the illuminated area is 5336 km^2 including the spill-over area. In these conditions, the value of μ considered in this study is 88%.
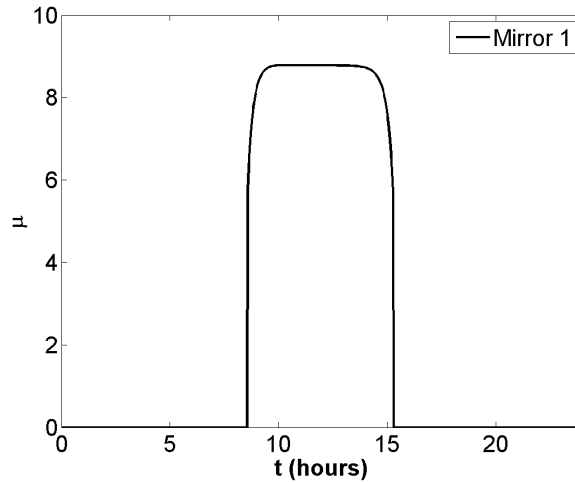

Figure 13. Loss factor due to the surface wrinkles of the mirrors.

The mirror reflectance coefficient (ρ) indicates the percentage of sunlight that is specularly reflected, therefore excluding scattered and absorbed light. This coefficient strictly depends on the material deposited on the substrate of the mirror to provide reflectivity. If the mirror is realized in space, it would be possible to consider Sodium for the reflective layer that would provide a reflectivity coefficient of 0.99 [12] . However, Sodium is unstable in the atmosphere and for this reasons other materials like silver or aluminium are examined for this task with reflectivity coefficients of 0.98 and 0.92, respectively. The material commonly considered for this purpose is Aluminium, mainly because is inexpensive, lightweight and durable.

With regard to the solar farm, currently, the efficiency of a solar cell (ϵ_{PV}) made of silicon is approximately 20%; however, when multi-junction solar cells based on more expensive materials such as gallium arsenide or indium selenide, the overall efficiency can be as high as $31 - 32\%$. This number can be further increased up to 35% (46% in lab conditions) when concentrating optics are employed through Concentrator Photovoltaics (CPV): these systems use lenses and curved mirrors to focus sunlight onto small highly-efficient multi-junction solar cells. In this study ϵ_{PV} is set to 40%.

Finally, the coverage ratio efficiency (ϵ_{GCR}) indicates how much of the overall area of solar farm is actually covered with solar panels (area of the PV modules divided by the overall area of the solar farm). Generally, solar panels are tilted depending on the latitude in order to maximize the amount of energy received. As the tilt angle increases, GDR must decrease to prevent reductions in energy capture due to shading. Again, the equatorial regions are the most advantageous locations because a larger tilting angle is required for solar farms at high latitudes and a minimum tilt

18

angle is used for the equator. Therefore, ϵ_{GCR} is set to 80% in this analysis.

Included in the losses caused by natural conditions are the atmospheric transmittance (τ) and cloud coverage (ψ). The transmittance factor of the reflected light travelling through the atmosphere between the mirror and the solar farm on the ground is given, according to Reference 19, as:

$$\tau = 0.1283 + 0.7559e^{-0.3878\ sec\left(\frac{\pi}{2}-\epsilon\right)} \tag{27}$$

where ϵ is the elevation angle measured at the solar farm location (see Figure 5). Computing Eq. (27) for both mirrors when they are visible from the solar farm on the ground τ is found to be roughly 64% for both mirrors. If the coefficient of scattered transmittance is considered as well (6%), the overall transmittance at sea level is $\tau = 70\%$. Finally, regarding the cloud cover factor (ψ), it depends on the latitude and the Equatorial regions occurs to be less covered by clouds all over the year. Moreover, large beams are less attenuated with respect to smaller beams delivered for example by low Earth orbits. In this case, the delivered beams of light are approximately $110\ km$ in diameter. For these reasons a cloud cover factor of 90% is considered in this study.

Therefore, considering all loss factors and Eq. (23), it can be seen that the final energy produced depends on the dimensions of the mirrors and the solar farms. As can be seen in Eq. (20) the illuminated area does not depend on the dimensions of the mirrors but only on its position in space (slant range (y) and elevation angle (ϵ)) and their average values are in the range $4931 - 8753\ km^2$. In Table (3), the results of the energy produced by the three solar farms are reported for several values of the area of the mirror and the solar farms.

Table 3. Total energy generated per day from the three solar power farms on the ground for several sizes of the mirrors and the solar farms.

D_m (km)	A_m (km²)	Mass (T)	A_{SP} (km²)	E_{totSP1} (GWh)	E_{totSP2} (GWh)	E_{totSP3} (GWh)
1.13	1	6.67	100	0.0092	0.0090	0.0095
2.52	5	33.33	100	0.046	0.045	0.047
3.57	10	66.67	100	0.092	0.091	0.095
6.18	30	200	100	0.28	0.27	0.28
7.97	50	333.33	100	0.46	0.45	0.47
11.28	100	666.67	100	0.92	0.91	0.94
6.18	30	200	200	0.55	0.54	0.57
7.97	50	333.33	200	0.92	0.91	0.95
7.97	50	333.33	300	1.38	1.34	1.42
7.97	50	333.33	500	2.30	2.26	2.37
11.28	100	666.67	500	4.60	4.53	4.74

In particular, the first 6 rows in Table (3) show the energy produced (GWh) by mirrors of several dimensions ($1 - 100 \ km^2$) and solar farms of $100 \ km^2$. Considering a mirror of $50 \ km^2$ and $200 \ km^2$ solar farms, Figures 14 and 16 can be obtained.
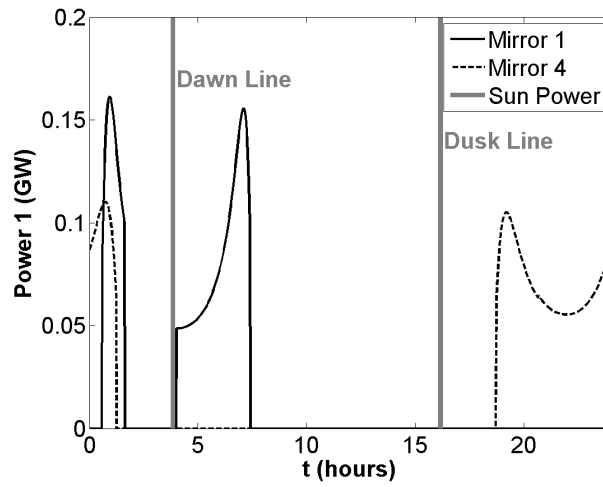

Figure 14. Distribution of the power (GW) generated in a day by the solar farm in central Africa.
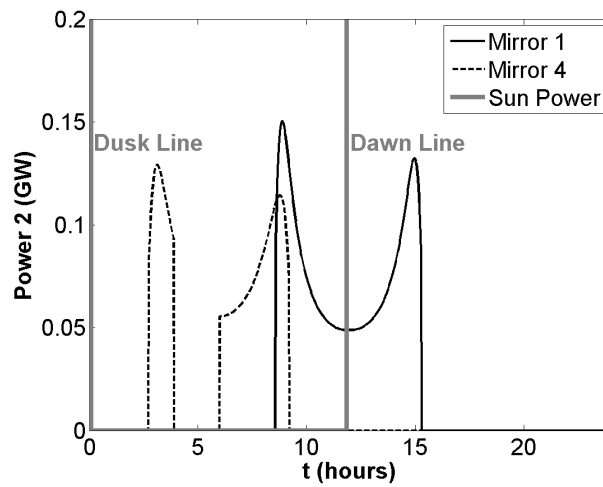

Figure 15. Distribution of the power (GW) generated in a day by the solar farm on the Pacific Coast.
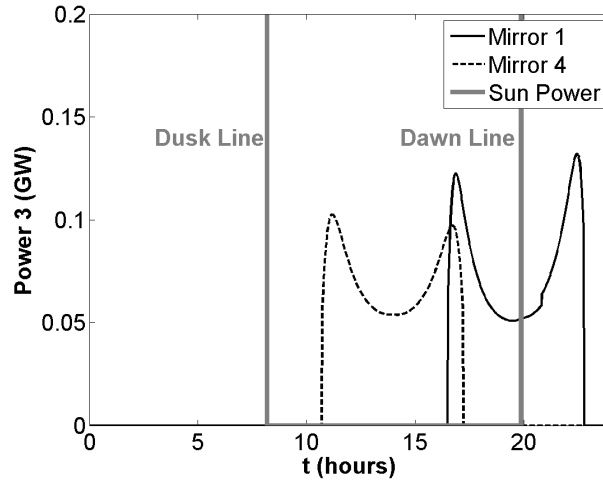
Figure 16. Distribution of the power (GW) generated in a day by the solar farm in Oceania.

The figures represent the distribution of the power in GW generated in a day by each solar farm. In particular, the effect of both mirrors and the eclipse time are taken into account. The shape of the curves is due to the elliptical orbit of the mirrors. The distance of the mirrors in space with respect to the solar farms changes greatly along the orbit: the power generated is lower when the mirror is at the apogee. The distance y appears to be the most significant term in the computation of Eq. (23). Moreover, in Figures 14 and 15 the effect of the eclipse can be noted: the first mirror is in eclipse from $1.40\ AM$ to $3.58\ AM$ while is orbiting above the solar farm in central Africa, whereas the second mirror is over-shaded by the Earth between $3.53\ AM$ and $5.58\ AM$, when it is above the Pacific Coast.

In the figures, local dawn/dusk lines are reported to show the duration of the day. Data is obtained considering the annual average of the solar angle above the location (data from Archive of Surface meteorology and Solar Energy, John M. Kusterer, NASA Langley ASDC User Services). As can be seen in the figures above, in all the three cases the first mirror provide energy for three hours after dawn. However, despite the sun already rose, it can be demonstrated that in the first three hours of sunlight, the Sun is only 20-30° (depending on the season) above the horizon; therefore, the energy supplied by the mirror is still rather advantageous for the solar farms. Despite the energy produced through the two space mirrors can be as high as $4.74\ GWh$ per day (see Tab. 3), the maximum flux (W/m^2) reaching the surface every day is estimated to be only the 3% of normal daylight. This estimation is obtained considering the best case scenario where the maximum quantity of energy is received.

CONCLUSION

A constellation of two large space mirrors (area-to-mass ratio $150\ m^2/kg$) is considered to provide three solar farms on the ground with additional solar power during the night or peak hours (evening and early morning). Through the basic concepts of the theory of flower constellations, the semi-major axis and other orbital elements such as the

21

RAAN and the mean anomaly are chosen so that the constellation has a repeat ground track and each mirror completes 3 orbits per day. The starting configuration for the constellation consisted of four mirrors; however, only two of them have been selected and further investigated because their orbits appear to be mostly on the dark side with respect to the Sun. These orbits are also called "Sun-perigee pointing" because the perigee points always towards the Sun. This means that the mirrors spend most of their time near apogee and orbiting above the areas of interest during the night. This feature is exploited to select the orbits of interest and reduce the configuration to only two space mirrors. These orbits maintain their shape in space and provide a repeat ground track if perturbations are neglected. However, the space mirrors are high area-to-mass ratio objects and, therefore, perturbations due to solar radiation pressure are important. Thus, Reference 4 and 8, where the effect of oblateness and SRP are exploited to find suitable frozen orbits, are considered.

The solar radiation pressure that the mirrors are subject to depends strictly on the incident angle and, in other words, on the orientation of the mirror with respect to the Sun. For this reason it is related to the steering law adopted for the mirror. In this paper, two different steering laws are considered. The first entails that the mirror points towards the centre of the Earth, whereas the second steering law considers the track of each solar farm while the mirrors satisfy the visibility conditions. The first steering law is rather straightforward and provides a useful starting approach for the development of the second law. The second steering law is more complex, the solar farms have to be exactly under the apogee of the orbits in order to assure that the mirror receives the same SRP along the orbit and its final balance is zero. In this way, the perturbations of J_2 and SRP are counterbalanced and their effect on the semi-major axis and the eccentricity is null. The only parameter to be affected by the perturbations is the argument of the perigee this issue is exploited in order to control the variation of the apse line of the orbit and point always towards the Sun. The eccentricity of the orbits is chosen so that the apse line precesses at the same rate of the Sun. In this way, the perigee of the orbit always points towards the Sun.

Therefore, the second steering law represent a slight different but more accurate method to provide the solar farms with additional solar energy. Each mirror orbits above every solar farm every day. In particular, considering the local time at every location and the combination of the coverage of both mirrors, the solar farm in central Africa receives surplus energy from $7.50\ PM$ to $8.30\ AM$, the one on the Pacific coast from $11.40\ PM$ to $12.20\ PM$ and the third solar farm located in Oceania between $6.40\ PM$ and $6.45\ AM$. Each mirror is in eclipse once per day, the first mirror is over-shaded by the Earth for $2h\ 21'$ while it is above central Africa and the second mirror for $2h\ 5'$ while orbiting above the Pacific coast. Considering the eclipse time, the total coverage time for the solar farm in central Africa is 11 hours, for the solar farm in the Pacific coast is $10h\ 55'$ and for the solar farm in Oceania is $13h\ 13'$. Considering the loss factors due to the quality of the mirror, the efficiency of the solar farm and natural conditions, the total energy generated depends on both the dimensions of the mirrors and solar farms. Considering, for example, three solar farms of $200\ km^2$ and two $50\ km^2$ parabolic mirrors, the total additional energy delivered each day is $0.92\ GWh$ in central

22

Africa, $0.91\ GWh$ for the solar farm on the Pacific coast and $0.95\ GWh$ for the third farm in Oceania.

ACKNOWLEDGMENT

REFERENCES

[1] L. M. Fraas, B. Derbes, and A. Palisoc, "Mirrors in Dawn Dusk Orbit for Low-Cost Terrestrial Solar Electric Power in the Evening," *51st AIAA Aerospace Sciences Meeting including the New Horizons Forum and Aerospace Exposition*, 2013, p. 1191.

[2] K. A. Ehricke, "The extraterrestrial imperative," *Futures*, Vol. 13, No. 2, 1981, pp. 107 – 114, http://dx.doi.org/10.1016/0016-3287(81)90018-5.

[3] L. M. Fraas, "Mirrors in space for low-cost terrestrial solar electric power at night," *Photovoltaic Specialists Conference (PVSC), 2012 38th IEEE*, IEEE, 2012, pp. 002862–002867.

[4] C. Colombo, C. Lucking, and C. R. McInnes, "Orbital dynamics of high area-to-mass ratio spacecraft with J2 and solar radiation pressure for novel Earth observation and communication services," *Acta Astronautica*, Vol. 81, No. 1, pp. 137 – 150, http://dx.doi.org/10.1016/j.actaastro.2012.07.009.

[5] L. Broglio, "Una Politica Spaziale per il Nostro Paese, Prospettive del Progetto San Marco: Il Sistema Quadrifoglio," *Centro di Ricerca Progetto San Marco, Internal Report*, 1981.

[6] M. Ruggieri, M. Sanctis, T. Rossi, M. Lucente, D. Mortari, C. Bruccoleri, P. Salvini, and V. Nicolai, "The Flower Constellation Set and its Possible Applications," *ACT Final report, Aridana*, Vol. 5, 2008, p. 4108.

[7] M. P. Wilkins, C. Bruccoleri, and D. Mortari, "Constellation design using flower constellations," *Space Flight Mechanics Meeting Conference*, 2004-Feb.-9-13, pp. 04–208.

[8] R. Bewick, C. Lücking, C. Colombo, J. Sanchez, and C. McInnes, "Heliotropic dust rings for Earth climate engineering," *Advances in Space Research*, Vol. 51, No. 7, 2013, pp. 1132–1144.

[9] R. Bewick, J.-P. Sanchez Cuartielles, and C. McInnes, "Use of orbiting reflectors to decrease the technological challenges of surviving the lunar night," *62nd International Astronautical Congress 2011*, 2011, pp. number 33360–IAC.

[10] U. Walter, *Astronautics: the physics of space flight*. John Wiley and Sons, 2012.

[11] R. S. L. Ortizlongo, Carlos R, "Method for the calculation of spacecraft umbra and penumbra shadow terminator points," *Tech. Rep. 3547, Lyndon B. Johnson Space Center, Houston,Tex, USA*, 1995.

[12] A. J. J. L. Canady Jr, John E, "Illumination from space with orbiting solar-reflector spacecraft," *NASA*, No. TP–2065, 1982.

[13] C. R. McInnes, M. MacDonald, V. Angelopolous, and D. Alexander, "GEOSAIL: exploring the geomagnetic tail using a small solar sail," *Journal of Spacecraft and Rockets*, Vol. 38, No. 4, 2001, pp. 622–629.

[14] C. R. McInnes, *Solar sailing: technology, dynamics and mission applications*. Springer Science and Business Media, 2013.

[15] J. Wertz and W. Larson, *Space Mission Analysis and Design*. Space Technology Library, Springer Netherlands, 1999.

[16] O. Mori, Y. Shirasawa, Y. Mimasu, Y. Tsuda, H. Sawada, T. Saiki, T. Yamamoto, K. Yonekura, H. Hoshino, J. Kawaguchi, *et al.*, "Overview of IKAROS mission," *Advances in Solar Sailing*, pp. 25–43, Springer, 2014.

[17] A. Borggräfe, J. Heiligers, M. Ceriotti, and C. R. McInnes, "Shape control of slack space reflectors using modulated solar pressure," *Proc. R. Soc. A*, Vol. 471, The Royal Society, 2015, p. 20150119.

[18] S. Potter and D. Davis, "Orbital reflectors for space solar power demonstration and use in the near term," *AIAA SPACE 2009 Conference and Exposition. California: AIAA*, 2009.

[19] H. C. Hottel, "A simple model for estimating the transmittance of direct solar radiation through clear atmospheres," *Solar Energy*, Vol. 18, No. 2, 1976, pp. 129–134.